Neutron Reflectometry Simulation of Thin Film Heterostructures with Ferromagnetic and Superconducting Layers

Reiner Ramos-Blazquez[a]*, Claudia Garcia-Rodriguez[b], Adolfo Collado-Hernandez[c]

[a] *Facultad de Ciencias Físico Matemáticas, Universidad Autónoma de Nuevo León, Av. Universidad s/n, San Nicolas de los Garza, Nuevo León, México. ORCID: https://orcid.org/0009-0008-6274-7640*
[b] *Facultad de Ciencias Físico Matemáticas, Universidad Autónoma de Nuevo León, Av. Universidad s/n, San Nicolas de los Garza, Nuevo León, México. ORCID: https://orcid.org/0009-0006-2849-3662*
[c] *Facultad de Ciencias Físico Matemáticas, Universidad Autónoma de Nuevo León, Av. Universidad s/n, San Nicolas de los Garza, Nuevo León, México. ORCID: https://orcid.org/0009-0004-3440-8378*
**email: rramos9708@gmail.com*

Recibido 17 de marzo de 2025, Aceptado 15 de abril de 2025

Resumen

En este trabajo, resolvemos la ecuación de Schrödinger para simular la interacción de neutrones con películas delgadas en el contexto de la técnica de Reflectometría de Neutrones. Estudiamos las curvas de reflectividad de una estructura compuesta por materiales superconductores a ambos lados de una capa ferromagnética. La muestra analizada tiene la configuración Nb (15 nm) / V (70 nm) / X (3 nm) / Nb (100 nm), donde X representa la capa ferromagnética, específicamente Fe, Ni o Gd. Analizamos la dependencia de las curvas de reflectividad con el ángulo de incidencia para ciertos rangos de longitud de onda y discutimos las tendencias observadas. Además, simulamos curvas de Reflectometría de Neutrones Polarizados y comparamos los resultados para diferentes posibles orientaciones de la magnetización de la muestra, verificando las simulaciones con los resultados esperados. Por último, comparamos las curvas de reflectividad para diferentes materiales ferromagnéticos y explicamos los patrones resonantes y correlacionados observados entre las curvas de reflectividad y absorción. Estos efectos se atribuyen a un aumento de la densidad de neutrones cerca de la capa de gadolinio, particularmente cuando el antinodo de la onda estacionaria coincide con esta cada para longitudes de onda de "resonancia".

Palabras clave: *reflectometría, neutrones, películas delgadas, ferromagnético, superconductividad*

Abstract

In this work, we solve the Schrödinger equation to simulate the interaction of neutrons with thin films in the context of Neutron Reflectometry. The reflectivity curves of a structure composed of superconducting materials on both sides of a ferromagnetic layer was studied. The sample under investigation has the configuration Nb (15 nm) / V (70 nm) / X (3 nm) / Nb (100 nm), where X represents the ferromagnetic layer, specifically Fe, Ni or Gd. The dependence of the reflectivity curves on the angle of incidence for different wavelengths was analyzed and the resulting trends were discussed. Additionally, we simulated Polarized Neutron Reflectometry curves and compared the results for different orientations of the sample's magnetization, verifying the simulations with the expected behaviors. The reflectivity curves for different ferromagnetic materials were also compared. Lastly, the observed resonant and correlated patterns between reflectivity and absorption curves were explained. These effects are attributed to an enhancement of the neutron density near the gadolinium layer, particularly when the antinode of the standing wave coincides with the layer at specific "resonant" wavelengths.

Keywords: reflectometry, neutrons, thin films, ferromagnetic, superconductivity

Introduction

As is well known and was confirmed during the 1920s, light exhibits a wave-particle duality. It behaves like a wave in phenomena such as diffraction and interference, and like a particle in effects such as the photoelectric and Compton effects. Louis de Broglie proposed that this nature might also apply to matter. He introduced the relationships between "particle- like" quantities, such as energy E and momentum $\vec{p}$, and "wave-like" quantities such as frequency w and the wave vector $\vec{k}$:

$$E = h\nu = \hbar w,\ \vec{p} = \hbar\vec{k},\quad p = \frac{h}{\lambda} \qquad (1)$$

The existence of the neutron was confirmed afterward by James Chadwick (1891-1974), who identified it as a neutral particle emitted during alpha particle bombardment of beryllium.

In 1932 James Chadwick (1891-1974) discovered the existence of the neutron by bombarding a sheet of beryllium with alpha particles.

The wave-particle duality allows neutrons to exhibit such behavior at the interface between two media: neutrons are reflected and refracted at the boundary of two materials with different refractive indices. This also leads to interference phenomena, creating a pattern in the reflectivity profile that is directly related to the thickness of the films. Neutron interaction with matter occurs with the atomic nucleus, enabling contrast tuning through isotopic substitution [1].

Neutron Reflectometry is a powerful technique for investigating both non-magnetic and magnetic samples, providing detailed information on the thickness, roughness, and density profiles of thin films [2]. In the case of magnetic materials, Polarized Neutron Reflectometry (PNR) utilizes the neutron's spin to probe magnetic depth profiles. Recently, PNR has been employed to explore the interplay between ferromagnetism, superconductivity and helimagnetism in thin film heterostructures [3-9].

Neutron Reflectometry is a valuable technique for analyzing the coverage and conformation of anchored and adsorbed polymers at liquid/thin film interfaces [10, 11]. Operando neutron reflectometry measurements have been performed to study the insertion of lithium into amorphous silicon film electrodes [12]. Specular neutron reflectometry has also been applied to investigate the kinetics and dynamics at air/water interfaces [13].

The detection and quantification of hydrogen has become increasingly important in research on electronic materials and devices, as hydrogen content is now recognized as a critical parameter influencing electronic properties. Resonant neutron reflectometry is used for hydrogen detection [14].

Additionally, ion distribution in dry polyelectrolyte multilayers has been studied, where fitting to the experimental data enabled the determination of the Scattering Length Density (SLD) profile [15].

Materials and methods

In Neutron Reflectometry, a collimated beam is directed to the sample surface at an angle α_i and is reflected from the surface at angle α_f (see Figure 1).

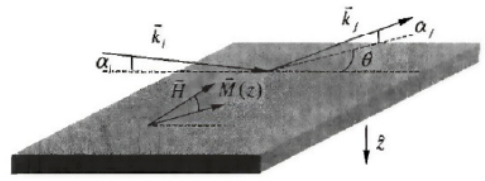

Figure 1. Reflection of a neutron beam on a surface, α_i is the angle of incidence and α_f is the angle of reflection.

The intensity of the reflected beam, measured as a function of wavelength reveals information about in-depth chemical and magnetic profiles. If the surface is corrugated, or if the material lacks lateral uniformity, deviations from specular reflection occur, either in the reflection plane ($\alpha_i \neq \alpha_f$) or out of it ($\theta \neq 0$). The case of specular reflection is the simplest to treat.

Neutron reflectometry assumes completely elastic scattering of neutrons: $|\overrightarrow{k_f}| = |\overrightarrow{k_i}| = {}^{2\pi}/_{\lambda}$.

$$Q_x = k_{fx} - k_{ix} = {}^{2\pi}/_{\lambda}(cos\alpha_f - cos\alpha_i) \quad (2)$$

$$Q_z = k_{fz} - k_{iz} = {}^{2\pi}/_{\lambda}(sin\alpha_f + sin\alpha_i) \quad (3)$$

For specular reflection ($\alpha_i = \alpha_f$), the transferred momentum components are: $Q_x = 0$ y $Q_z = 2k_z = {}^{4\pi}/_{\lambda} sin\alpha$.

In this case, only the perpendicular component (along $\hat{z}$) of the wavevector is influenced by the sample's potential, which can be modeled as a depth-dependent potential. Thus, we can represent the neutron as a particle with kinetic energy $\hbar^2 k_z^2/2m$, hitting a potential of height U(z).

In practice a range of Q_z is spanned either by changing the wavelength, and keeping fixed the angle of incidence, or by changing the angle of incidence at fixed wavelength. The use of polarization devices, such as polarizing mirrors and spin flippers, allows control and analysis of the neutron spin. Conventionally, the direction of initial polarization is fixed. Spin states before and after reflection are used to define four reflectivity channels: R^{++}, R^{--}, R^{+-}, and R^{-+}, where the signs indicate the polarization of the neutron relative to the reference magnetic field.

Accurate interpretation of reflectivity data requires comparison with theoretical predictions based on a model of the sample. This involves solving the neutron wave equation across the material's interfaces, considering the potential landscape experienced by the neutron.

A free neutron is represented by a plane wave:

$$\psi_0(\boldsymbol{r},\boldsymbol{k},t) = \exp(i\boldsymbol{kr} - iwt) \quad (4)$$

In this expression, **k** is the wave vector, which corresponds to the momentum **p** (**k**=p/ħ), while the frequency ω is linked to the neutron's kinetic energy $E=p^2/2m$ ($w=E/\hbar$) where m is the neutron mass. This plane wave is a solution to the free particle Schrödinger equation:

$$i\hbar\frac{\partial\psi}{\partial t} = -\frac{\hbar^2}{2m}\Delta\psi \quad (5)$$

Equation (5) is valid only in empty space, but when the neutron encounters matter, the equation must be modified to account for the interaction potential:

$$i\hbar\frac{\partial\psi(\boldsymbol{r},t)}{\partial t} = \frac{\hbar^2}{2m}[-\Delta + u(\boldsymbol{r},t)]\psi(\boldsymbol{r},t) \quad (6)$$

Here, the term $\hbar^2 u/2m$ represents the effective potential experienced by the neutron due to the medium. In general, the solution to this equation is not a plane wave. We will focus on time-independent potentials and systems that vary along only one spatial dimension, typically the x-axis. This reduces the problem to the one-dimensional equation:

$$\left[\frac{d^2}{dx^2} - u(x) + k_x^2\right]\psi(x) = 0 \quad (7)$$

Where $k_x = \sqrt{k^2 - k_{ll}^2}$ represents the component of the wave vector perpendicular to the surface.

The optical potential is given by:

$$U = \frac{\hbar^2}{2m}4\pi N_0 b_c \quad (8)$$

where $\hbar=h/2\pi=1.05*10^{-34}$Js is the reduced Planck constant, $m=1{,}675*10^{-24}$ g is the neutron mass, $N_0\approx10^{23}cm^{-3}$ is the number of atoms per unit volumen of the medium, and b_c is the average (coherent) neutron scattering amplitude of a single atomic nucleus. The reduced potential $u_0=2mU/\hbar^2$ used in the equations above is equal to $4\pi N_0 b_c$. Note that the scattering amplitude varies across different materials and may be either positive or negative.

To describe reflection and transmission for arbitrary potentials, consider a system composed by some potential u_i (i=1,2), and the corresponding reflection and transmission amplitudes denoted by r_i and t_i [16]. The goal is to determine the overall reflection R_{12} and transmission T_{12} amplitudes. Assume that a plane wave $\exp(ik_x x)$ is incident on the first mirror from the left with amplitude 1 at the surface of the first mirror. The wave incident on the second mirror has amplitude X at its surface (Figure 2.). The equation for X is:

$$X = t_1 + r_1 r_2 X \quad (9)$$

The solution of Eq. (9) is:

$$X = \frac{t_1}{1-r_1 r_2} \quad (10)$$

The total transmission and reflection amplitudes can be represented:

$$R_{12} = r_1 + t_1 r_2 X \quad (11)$$

$$T_{12} = t_2 X \quad (12)$$

Substituting Eq. (10) in Eq. (11) and Eq. (12) we obtain:

$$R_{12} = r_1 + t_1^2\frac{r_2}{1-r_1 r_2}\ , \quad T_{12} = \frac{t_2 t_1}{1-r_1 r_2} \quad (13)$$

Although the resulting expressions are relatively straightforward, they reveal a fundamental conclusion: any complex potential can be virtually divided at an arbitrary point into two separate regions. The total reflection and transmission amplitudes of the system can be derived from the individual scattering amplitudes of these regions.

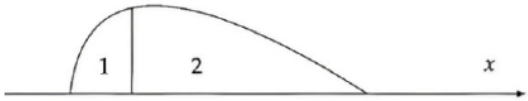

Figure 2. At any point every potential can be subdivided into two parts.

The above can be expressed mathematically as follows:

$$r(d_1+d_2) = r(d_1) + t(d_1)\frac{\mathrm{r}(d_2)}{1-\mathrm{r}(d_1)\mathrm{r}(d_2)}t(d_1) \quad (14)$$

$$t(d_1+d_2) = \frac{t(d_1)\mathrm{t}(d_2)}{1-\mathrm{r}(d_1)\mathrm{r}(d_2)} \quad (15)$$

If we consider three potentials:

$$r[d_1+(d_2+d_3)] = r(d_1) + t(d_1)\frac{\mathrm{r}(d_2+d_3)}{1-\mathrm{r}(d_1)\mathrm{r}(d_2+d_3)}t(d_1) \quad (16)$$

$$t[d_1+(d_2+d_3)] = \frac{t(d_1)\mathrm{t}(d_2+d_3)}{1-\mathrm{r}(d_1)\mathrm{r}(d_2+d_3)} \quad (17)$$

Equations (14) and (15) are the basis of an iterative algorithm in which the theoretical model is centered, in this expression it is necessary to consider the presence of the spin. The square of the modulus of 14 (15) in its last iteration gives us the reflectivity (transmissivity) of the sample.

Results and Discussion

Based on the equations presented in the previous section, we used MATLAB to simulate the reflectivity and absorption curves resulting from interaction of neutrons with the structure: Nb (15nm) / V (70nm) / X (3nm) / Nb (100nm) onto a Al_2O_3 substrate. In this multilayer system, vanadium and niobium act as superconducting materials, with bulk critical temperatures of approximately 5.4 K and 9.4 K, respectively. X is a ferromagnetic material, we use X=Fe, Gd, Ni.

3.1. Dependence of Reflectivity with the incidence angle.

In Figure 3. the dependence of the reflectivity (in the absence of magnetization) on wavelength is analyzed as a function of the angle of incidence for the structure Nb (15nm) / V (70nm) / Fe (3nm) / Nb (100nm). It can be observed that, for any given wavelength, the reflectivity is higher at smaller angles of incidence. This implies that, as the incident beam approaches a perpendicular orientation to the sample surface, the probability of other processes such as transmission or absorption increases.

Another detail to highlight in Figure 3. is the increase in the critical wavelength at which total reflection begins to occur.

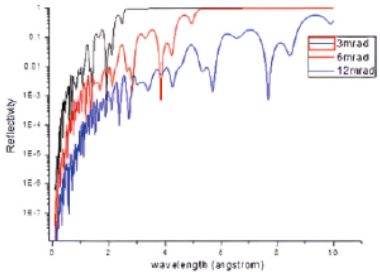

Figure 3. Neutron reflectivity curves for different incident angles.

3.2. Sample Magnetization Analysis

The behavior of the reflectivity curves is analyzed for different values of magnetization in the sample Nb (15nm) / V (70nm) / Gd (3nm) / Nb (100nm), considering both collinear and non-collinear configurations.

Let's analyze the three possible cases:

Caso 1: $M = 0 \rightarrow R^{++} = R^{--};\ R^{+-} = R^{-+} = 0$

Caso 2: $M \neq 0; B \parallel M \rightarrow R^{++} \neq R^{--};\ R^{+-} = R^{-+} = 0$

Caso 3: $M \neq 0; B \nparallel M \rightarrow R^{++} \neq R^{--};\ R^{+-} \neq 0;\ R^{-+} \neq 0$

In the first case, the sample is assumed to be not magnetized, so the non-spin flip reflectivities (R^{++} and R^{--}) are equal, and the spin flip components (R^{+-} and R^{-+}) are zero.

In the collinear case, the magnetization vector of the sample is aligned with the external magnetic field. In this configuration, the non-spin flip components differ, while the spin flip components remain zero.

In the non-collinear case, components of the magnetization vector are assumed to be perpendicular to the external field, introducing spin-flip contributions that make R^{+-} and R^{-+} non-zero.

Let's now analyze the collinear case with an angle of incidence of 6mrad. At $T>T_c$ magnetization is considered only in the Gd layer.

In figure 4., case 1 is analyzed, assuming the sample has no magnetization. Since $R^{SF} = 0$, the notation $R^{++}=R^{+}$ and $R^{--}= R^{-}$ is used. As shown, the reflectivity curves R^{+} and R^{-} coincide.

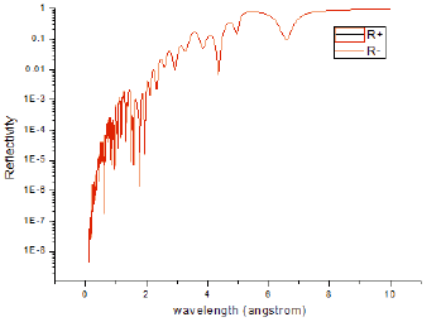

Figure 4. Neutron reflectivity for M(Gd)=0Oe.

In Figure 5., the reflectivity curve for M_z(Gd)=100 Oe is analyzed. For relatively small magnetization values such as this, the differences between the R^{+} and R^{-} reflectivity curves are barely noticeable. However, when considering a higher magnetization value, such as M_z(Gd)=10000 Oe, the differences between the two curves become more evident.

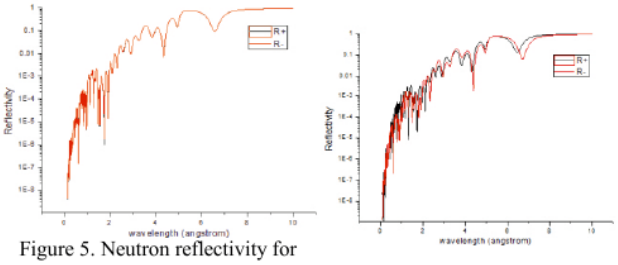

Figure 5. Neutron reflectivity for M_z(Gd)=100Oe (left) and M_z(Gd)=10000Oe (right).

Non-collinear case

Let us now add a magnetization component in a direction parallel to the sample plane: M_x(Gd) = 500 Oe and M_z (Gd) = 1000 Oe. The presence of the x-component allows a tendency for the neutron spin to align in this direction as well, which introduces the possibility of spin flips. As a result, the spin-flip R^{SF} components become non-zero and are approximately equal (see Figure 6.). If M_x(Gd) is increased to 10000 Oe, the values of R^{+-} and R^{-+} increase accordingly.

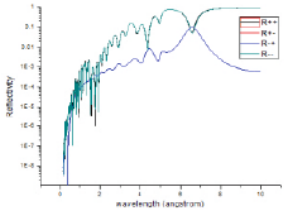

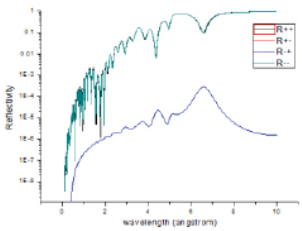

Figure 6. Neutron reflectivity for $M_z(Gd)=1000Oe$, $M_x(Gd)=100Oe$, $M_y(Gd)=0Oe$ (left) and for $M_z(Gd)=1000Oe$, $M_x(Gd)=10000Oe$, $M_y(Gd)=0Oe$ (right).

3.3. Reflectivity curves for different ferromagnets

Let's analyze the reflectivity curves (without considering magnetization and at an incidence angle of 6mrad) for the structure Nb (15nm) / V (70nm) / X (3nm) / Nb (100nm) where X = Gd, Fe and Ni, all of which are ferromagnetic elements.

The reflectivity and absorption curves for these samples are shown in Figure 7.

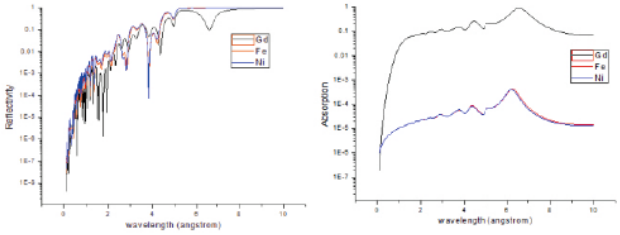

Figure 7. Neutron reflectivity (left) and absorption (right) for different ferromagnets.

The lower reflectivity for Gd compared to Fe and Ni is related to a considerably higher neutron absorption for Gd. The neutron absorption cross section for Gd is three orders of magnitude greater than for Fe and Ni.

3.4. Reflectivity and absorption for different thicknesses of the Gd layer

Now, let's compare the reflectivity and absorption curves for various thicknesses of the Gd (d_f) layer, considering $d_f = 3,6,9,12$ nm (see Figure 8.).

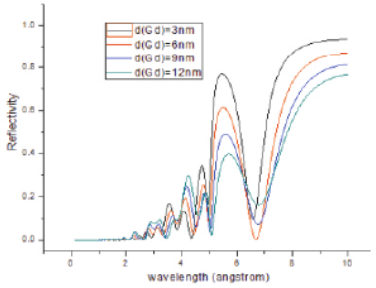

Figure 8. Neutron reflectivity for different Gd thickness.

As shown in the graph, the reflectivity curves decrease with increasing Gd thickness. This effect can be attributed to enhanced neutron capture by gadolinium. To verify this, Figure 9. presents the absorption curves for these thicknesses, showing a noticeable increase in absorption as the Gd layer becomes thicker.

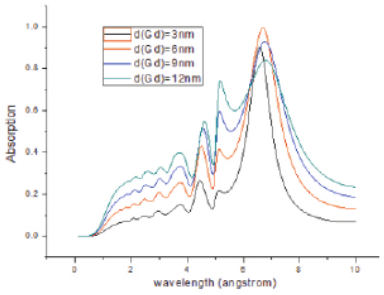

Figure 9. Neutron absorption for different Gd thickness.

Figure 10. displays both the reflectivity and absorption curves for the structure considering Gd ($d_f = 6$nm).

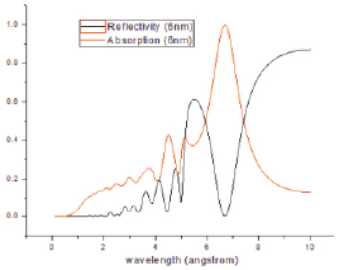

Fig. 10. Reflectivity and neutron absorption for d(Gd)=6nm.

The observed dependencies exhibit a resonant nature and show a clear correlation: a reduction in the reflectivity coincides with an increase in neutron absorption. This proves that the minimums in the neutron's reflection coefficient are due to their absorption. The resonant behavior can be attributed to an enhancement in the neutron density near the gadolinium layer, particularly when the standing wave's antinode aligns with this layer at specific "resonance" wavelengths [17].

Conclusions

The discussion of the results leads to the following conclusions regarding the properties of the Nb (15 nm) / V (70 nm) / X=Fe, Ni or Gd (3 nm) / Nb (100 nm), structure using Neutron Reflectometry simulations. For a given wavelength, the reflectivity is higher at smaller angles of incidence, indicating that as the incident beam approaches a perpendicular orientation relative to the sample surface, the likelihood of other processes such as transmission or absorption increases. The use of Gd as the ferromagnetic material results in significantly higher neutron absorption compared to Fe or Ni, due to the neutron absorption cross section of Gd being approximately three orders of magnitude greater than that of Fe and Ni. The minimum observed in the reflectivity curves are primarily attributed to neutron absorption by the Gd layer. Furthermore, the absorption curve exhibits a resonant behavior associated with an enhanced neutron density in the Gd layer at specific

wavelengths. This enhancement occurs when the antinode of the standing wave coincides with the position of the Gd layer, resulting in increased absorption under these specific "resonance" conditions.

References

[1] Cousin, F., Fadda, G. An introduction to neutron reflectometry. EPJ Web of Conferences 236 (2020) 04001. https://doi.org/10.1051/epjconf/202023604001

[2] Doucet, M., Archibald, R., Heller, W. Machine learning for neutron reflectometry data analysis of two-layer thin films. Mach. Learn.: Sci. Technol. **2** (2021) 035001. https://doi.org/10.1088/2632-2153/abf257

[3] Khaydukov, Y. Neutron reflectometry studies of Gd/Nb and $Cu_{30}Ni_{70}$/Nb superlattices. Journal of Physics: Conference Series 1389 (2019) 012060. https://doi.org/10.1088/1742-6596/1389/1/012060

[4] Nikitenko, Y., Zhaketov, V. Magnetism in Ferromagnetic-Superconducting Layered Structures. Physics of Particles and Nuclei, 2022, Vol. 53, No. 6, pp. 1089–1125. https://doi.org/10.1134/S1063779622060065

[5] Khaydukov, Y. et. al. On the feasibility to study inverse proximity effect in a single S/F bilayer by polarized neutron reflectometry. Pis'ma v Zh. Eksper. Teoret. Fiz., 2013, Volume 98, Issue 2, 116–120. https://doi.org/10.7868/S0370274X13140117

[6] Nagy, B. et. al. On the explanation of the paramagnetic Meissner effect in superconductor/ferromagnet heterostructures. EPL, 116 (2016) 17005. https://doi.org/ 10.1209/0295-5075/116/17005

[7] Ovsyannikov, G. et. al. Magnetic Proximity Effect at the Interface between a Cuprate Superconductor and an Oxide Spin Valve. Journal of Experimental and Theoretical Physics, 2016, Vol. 122, No. 4, pp. 738–747. https://doi.org/10.1134/S1063776116040063

[8] Andreeva, M. et. al. Nuclear Resonance Reflectivity of Dy/Gd Superlattices. JETP Letters, 2018, Vol. 107, No. 3, pp. 196–199. https://doi.org/10.1134/S0021364018030050

[9] Devyaterikov, D. et. al. Influence of Dimensional Effects on the Curie Temperature of Dy and Ho Thin Films. Physics of Metals and Metallography, 2021, Vol. 122, No. 5, pp. 465–471. https://doi.org/10.1134/S0031918X21050033

[10] Delcea, M., Helm, C. X-ray and Neutron Reflectometry of Thin Films at Liquid Interfaces. *Langmuir* 2019 *35* (26), 8519-8530. http://dx.doi.org/10.1021/acs.langmuir.8b04315

[11] Zhang, Z. et. al. Adsorption of non-ionic surfactant and monoclonal antibody on siliconized surface studied by neutron reflectometry. Journal of Colloid and Interface Science 584 (2021) 429-438. https://doi.org/10.1016/j.jcis.2020.09.110

[12] Jerliu, B. et. al. Lithium insertion into silicon electrodes studied by cyclic voltammetry and operando neutron reflectometry. Phys. Chem. Chem. Phys., 2018, 20,23480. https://doi.org/10.1039/C8CP03540G

[13] Campbell, R. Recent Advances in resolving Kinetic and Dynamic Processes at the Air/Water Interface using Specular Neutron Reflectometry. Current Opinion in Colloid & Interface Science Volume 37, September 2018, Pages 49-60. https://doi.org/10.1016/j.cocis.2018.06.002

[14] Guasco, L. et. al. Resonant neutron reflectometry for hydrogen detection. *Nat Commun* **13**, 1486 (2022). https://doi.org/10.1038/s41467-022-29092-z

[15] Ghoussoub, B. et. al. Ion distribution in dry polyelectrolyte multilayers: a neutron reflectometry study. Soft Matter, 2018,14, 1699-1708. https://doi.org/10.1039/c7sm02461d

[16] Utsuro, M., Ignatovich, V. (2010). Neutron Optics. John Wiley & Sons.

[17] Nikitenko, Y. Neutron Standing Waves in Layered Systems: Formation, Detection, and Application in Neutron Physics and for Investigation of Nanostructures. Physics of Particles and Nuclei, 2009, Vol. 40, No. 6, pp. 890–947. https://doi.org/10.1134/S1063779609060069